Strong and Stiff Aramid Nanofiber/ Carbon Nanotube Nanocomposites

Jiaqi Zhu,[†] Wenxin Cao,[†] Mingli Yue,[‡] Ying Hou,[‡] Jiecai Han,[*,†] and Ming Yang[*,‡]

[†]Center for Composite Materials and Structures and [‡]Key Laboratory of Microsystems and Micronanostructures Manufacturing, Harbin Institute of Technology, 2 Yikuang Street, Harbin 150080, People's Republic of China

ABSTRACT

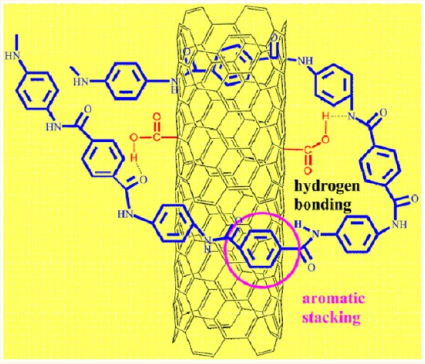

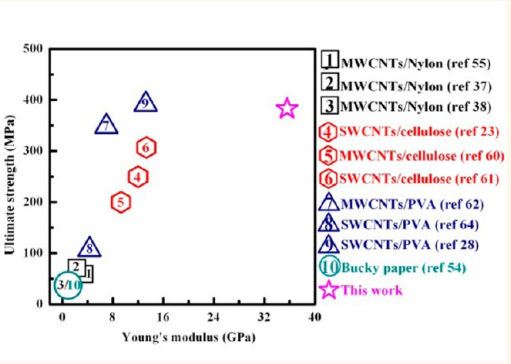

Small but strong carbon nanotubes (CNTs) are fillers of choice for composite reinforcement owing to their extraordinary modulus and strength. However, the mechanical properties of the nanocomposites are still much below those for mechanical parameters of individual nanotubes. The gap between the expectation and experimental results arises not only from imperfect dispersion and poor load transfer but also from the unavailability of strong polymers that can be effectively utilized within the composites of nanotubes. Aramid nanofibers (ANFs) with analogous morphological features to nanotubes represent a potential choice to complement nanotubes given their intrinsic high mechanical performance and the dispersible nature, which enables solvent-based processing methods. In this work, we showed that composite films made from ANFs and multiwalled CNTs (MWCNTs) by vacuum-assisted flocculation and vacuum-assisted layer-by-layer assembly exhibited high ultimate strength of up to 383 MPa and Young's modulus (stiffness) of up to 35 GPa, which represent the highest values among all the reported random CNT nanocomposites. Detailed studies using different imaging and spectroscopic characterizations suggested that the multiple interfacial interactions between nanotubes and ANFs including hydrogen bonding and $\pi-\pi$ stacking are likely the key parameters responsible for the observed mechanical improvement. Importantly, our studies further revealed the attractive thermomechanical characteristics of these nanocomposites with high thermal stability (up to 520 °C) and ultralow coefficients of thermal expansion (2−6 ppm·K^{-1}). Our results indicated that ANFs are promising nanoscale building blocks for functional ultrastrong and stiff materials potentially extendable to nanocomposites based on other nanoscale fillers.

KEYWORDS: nanotubes · CNTs · nanocomposites · mechanical properties · strength · stiffness · vacuum-assisted flocculation · layer-by-layer assembly · LBL · aramid nanofibers · CTE

Strong one-dimensional (1D) materials are of both fundamental and technical importance owing to their anisotropic structure, diverse compositions, and unique properties. From natural cellulose fibers and spider silk to the artificially developed carbon and polymer fibers (nylon, Kevlar, PBO, *etc.*), we see the tremendous and constant interest in the advance of novel strong 1D materials. Such research enthusiasm culminated in the discovery of carbon nanotubes (CNTs)[1] with intriguing mechanical properties (Young's modulus 1 TPa and strength 300 GPa).[2] Significant research attention has been attracted for the potential use of CNTs (mainly single-walled (SW) and multiwalled (MW)) as reinforcing fillers for polymeric composites.[3−5] The challenge in this field lies in the fact that the mechanical properties of these macroscale composites are still much below those for mechanical parameters of individual nanotubes.[6−8] The current resolution to this challenging problem focuses on improving attributes of the reinforcement phase to alleviate

* Address correspondence to hanjc@hit.edu.cn, yangm@hit.edu.cn.

Received for review September 2, 2014 and accepted February 24, 2015.

Published online February 24, 2015
10.1021/nn504927e

the dispersion problem and strengthen the interfacial interactions by for instance polymer functionalization and noncovalent grafting.[9−13] Other strategies include increasing the volume fractions and the aligning of CNTs.[14−20]

The design of high-performance nanocomposites will also benefit from the availability of novel polymeric matrices. According to the simple rule of mixture ($E_{composite} = E_{filler}V_{filler} + E_{matrix}V_{matrix}$, where $E_{composite}$, E_{filler}, and E_{matrix} are the material property of the composite, fillers, and the matrix, respectively; V_{filler} and V_{matrix} are the volume fraction of fillers and the matrix, respectively), it is quite reasonable to envision that if a good control over reinforcing phase can be complemented with polymeric matrices possessing superior mechanical properties, nanocomposites with exceptional mechanical properties will be realized. However, following this concept, some counterintuitive results have been observed. For example, replacement of poly(diallyldimethylammonium chloride) (PDDA) with a much stronger polysaccharide polycation (chitosan) (ultimate strength 108 MPa and stiffness 2 GPa) in clay nanocomposites unexpectedly resulted in lower strength and stiffness.[21] A comparable example was recently reported for composites using cellulose nanofibers as polymeric matrix, which have an intrinsic high strength (500 MPa) and stiffness (140−220 GPa).[22] It was however found that the addition of CNTs consistently weakened cellulose nanofiber films.[23] These observations, contrary to the predictions, unambiguously highlight the importance of finding innovative strong polymeric counterparts that can successfully match nanoscale fillers such as CNTs in the design of high-performance nanocomposites.

The present polymeric matrices for CNT-based nanocomposites include mostly thermosetting (such as epoxy) and thermoplastic polymers (such as PMMA).[3,4] These composite materials have been extensively studied using different procedures including melt processing,[24] *in situ* polymerization,[25] or solution blending.[26,27] However, the resultant composites still suffer from overall poor mechanical properties especially in strength and stiffness largely due to the low performance of polymeric matrices. Some impressive results have been achieved using hydrophilic polymers such as poly(vinyl alcohol) (PVA) by a layer-by-layer (LBL) assembly method.[28] However, the practical use of such materials may be affected by their water-wetting nature, which may result in the deterioration of mechanical properties due to the swelling effect.[29] Similar problems can be found in cellulose-based composite films.[30] While such an effect may be quite useful for the design of functional gradient materials[31] or environmental sensors,[32] it remains a challenge for applications where the consistence of mechanical performance is important.

The step toward the use of polymers with better intrinsic performance in the preparation of CNT-based nanocomposites has been taken with extensive work focusing on semicrystalline thermoplastic polymers such as aromatic polyether ketones, PEEKs (ultimate strength σ = 103 MPa and stiffness E = 3.8 GPa).[33] The largest enhancement was observed for PEEK composites incorporating 15 wt % chemical vapor deposited MWCNTs, where E increased up to 7.55 GPa.[34] Efforts toward the use of even stronger polymers with higher crystallinities have been shown to be successful in the preparation of nanocomposites, which however are mainly in the form of fibers. For example, Nylon-6- and PBO-based CNT composite fibers with enhanced mechanical properties have been obtained using spinning techniques.[35,36] However, such success does not necessitate the advance of composite films based on these strong synthetic polymers and CNTs, which are in fact very limited.[37,38] One of the possible reasons could be the reinforcement mechanism in these fibers such as the alignment of CNTs[16] and the kinetically frozen states with a lower degree of phase separation typically do not exist in the composite films. The robust structure of these crystalline polymers, which is usually accompanied by their sluggish chemical reactivity, brings additional difficulties in achieving synergetic effects when combining them with CNTs. A suitable system that allows the rational design of composite films based on strong synthetic polymers would be therefore much desirable and very likely result in record-high mechanical characteristics.

In an effort to explore the possibility of incorporating new polymeric building blocks into nanocomposites, we found that the dissolution of synthetic polymeric macrofibers in a DMSO KOH system resulted in the formation of a stable aramid nanofiber dispersion, which can be processed into thin films by LBL assembly.[39] We further demonstrated that aramid nanofibers (ANFs) can be used as reactive nanoscale materials for advanced composites with tailored mechanical properties.[40] ANFs are in essence the nanoscale version of polyparaphenylene terephthalamide (PPTA), a high-performance para-aramid polymer better known by its trade name, Kevlar, with exceptional mechanical performance (stiffness 109 GPa and strength 3.6 GPa).[41] Traditionally, Kevlar macrofibers are well-known components of personal armor and are widely used in composite materials to reinforce epoxy resins.[42] It would be very attractive to use Kevlar as a polymeric matrix in the preparation of composite materials considering its unique property combination of stiffness, strength, chemical and solvent resistance, thermooxidative stability, flame retardancy, and negative coefficient of thermal expansion (CTE).[43] Recently, there was some interesting work on the reinforcement of Kevlar macrofibers with CNTs using a solvent-swelling process,[44] and Kevlar-modified CNTs were also used to reinforce other polymers.[45,46] However, the use of Kevlar as a polymeric matrix in the preparation of

transparent CNT-based nanocomposites has never been reported.

In this work, the first example of transparent composite films made from ANFs and MWCNTs was demonstrated with record-high ultimate strength (σ = 383 MPa) and stiffness (E = 35 GPa) among all the reported nanocomposites using random distributed CNTs. In addition, the use of ANFs also lent composite films high-temperature stability and low CTE. Overall, our results showed that ANFs are promising strong nanoscale building blocks in polymeric nanocomposites with multiple intriguing properties.

RESULTS AND DISCUSSIONS

The tremendous interest in employing CNTs as fillers may necessitate a particular survey of the mechanical characteristics of the state-of-the-art polymeric nanocomposites. We intended to focus more on three systems including nylon/CNT, cellulose nanofiber (NF)/CNT, and PVA/CNT nanocomposites. The reason for selecting the first two systems is that they bear similarities with ANF/MWCNT nanocomposites: analogous with Kevlar, nylon is also a synthetic polymer (polyamide) widely used as high-performance fibers; for cellulose NFs, they have similar dimensions and comparable mechanical properties (E = 138 GPa and σ = 2 GPa) with ANFs. We also wanted to include a system within which we see the most remarkable mechanical properties. In this respect, recent studies have indicated that reinforcing PVA with CNTs has been shown to be the most successful. A summary of stiffness (E) and ultimate strength (σ) from these systems is included in Table S1 with data from other representative systems including bucky papers and recently developed graphene oxide (GO)-based nanocomposites[47−54] as well.

Nylon/CNT nanocomposites were usually prepared by melt or solution mixing.[24,37,38,55−58] The highest reported E and σ are 3.5 GPa[55] and 70 MPa,[37] respectively. These two records came from different systems, which could be attributed to the use of nylon with different chemical structures. However, the relatively low mechanical properties of nylon (σ = 35 to 220 MPa and E = 1.1 to 16 GPa) limited the overall performance of nylon-based nanocomposites. Different from nylon, cellulose NFs can be obtained from natural resources with appealing mechanical properties. Films made from nanocellulose have high E (13 GPa) and σ (223 MPa).[59] Unexpectedly, both E and σ of the cellulose NF/CNT composite films tended to decrease with increasing CNT contents.[23,60] A recent result demonstrated only a small improvement with a 3 wt % addition of CNTs: E is improved from 12.5 GPa to 13.3 GPa, and σ from 299 MPa to 307 MPa.[61] The most impressive results came from SWCNT/PVA nanocomposites made by LBL assembly with the demonstrated σ of 391.5 MPa and E of 15.6 GPa.[28] It is however noted that the content of SWCNTs in LBL assembled films is quite high, up to 70%, which would completely diminish the transparency of the polymeric matrix, a problem also for other strategies aiming at improving the contents of CNTs in the nanocomposites.[17,18] Interestingly, simple solution casting of PVA/CNT blends also gave remarkable results where the polymer−CNT interactions are completely noncovalent (van der Waals forces): σ of 348 MPa and E of 7.04 GPa can be achieved for a 0.6 vol % sample.[62] The surface modifications of CNTs using collagen,[63] hydroxyl groups,[64] and surfactants[65] have also been used in PVA/CNT nanocomposites to further improve the load transfer but with less dramatic effects.

Several points can be made based on the above summary: first, it is typically hard to achieve both high strength and stiffness in conventional nanocomposites, especially when using randomly distributed CNTs at low loading to keep good transparency; second, a polymer match with CNTs with suitable molecular structures and excellent mechanical properties would be much needed for the achievement of strong and stiff nanocomposites; third, always, effective stress transfer should be made possible by the enhanced interfacial interactions. In this context, the excellent mechanical properties of ANFs and the multiple interactions with functionalized MWCNTs enabled by their nanoscale dimensions can be very useful for addressing the challenge.

Mechanical Properties of ANF/MWCNT Nanocomposites. We employed a vacuum-assisted flocculation (VAF) method to prepare ANF/MWCNT nanocomposites (for details, see the Experimental Section and Supporting Information). X-ray diffraction (XRD) patterns confirmed the presence of both ANFs and MWCNTs in the composite films (Figure 1a,c). Importantly, the observed diffraction peaks of ANFs similar to that of Kevlar indicated the reservation of the crystalline PPTA structures in the nanoscale domains. The (110), (200), and (004) diffraction peaks of ANFs[39] can be detected, with the peak around $2\theta = 26°$ assigned to the diffraction from MWCNTs (Figure 1a).[66] Postannealing (200 °C in air for 1 h) was used to remove DMSO, which also improved the crystallinity of both the ANFs and composite films, as evidenced by the intensity increase of the diffraction peaks (Figure 1b). The crystallinity of ANFs does not change obviously upon the addition of more MWCNTs (Figure 1c). The thickness of the composite film as determined by SEM was found to be typically around 2 μm (Figure 1d) and can be used in calculating the mechanical properties. The pure ANF film showed an ultimate strength (σ) of 179.6 $\pm$ 6.2 MPa and stiffness (E) of 12.7 $\pm$ 0.8 GPa (Figure 2a,b). The additions of MWCNTs have obviously reduced the ultimate strain of the ANF film (Figure 2a). The 1.5 wt % addition of MWCNTs improved σ to 252.2 $\pm$ 8.6 MPa and E to 23.6 $\pm$ 1.4 GPa (Figure 2a,b). The increase of MWCNT loading to 2.5 wt % resulted in further improvement

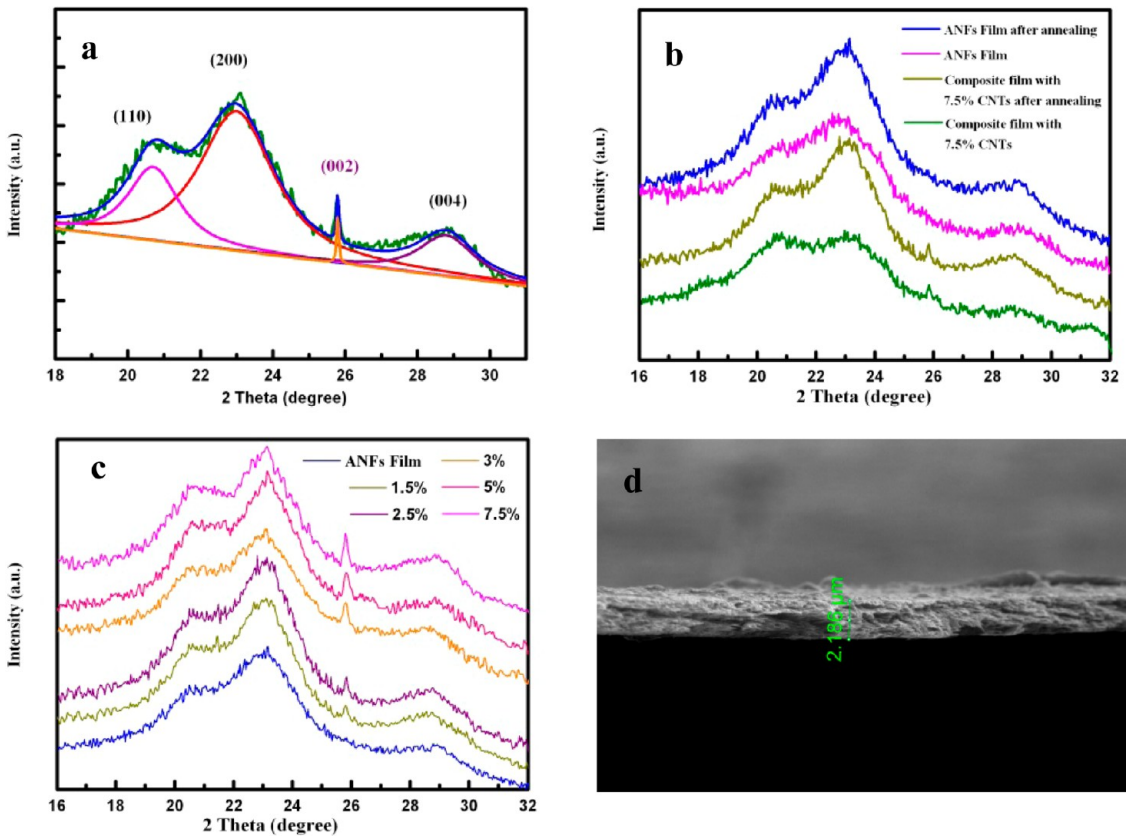

Figure 1. (a) XRD pattern of a composite film with 7.5 wt % MWCNTs with Gaussian fitting; (110), (200), and (004) diffraction peaks can be assigned to ANFs, and the (002) diffraction peak belongs to MWCNTs; (b) the evolution of XRD patterns upon annealing; (c) XRD patterns of composite films with different amounts of MWCNTs after annealing; (d) cross-sectional SEM image of a composite film with 7.5 wt % MWCNTs.

of σ to 361.2 $\pm$ 9.3 MPa and E to 34.4 $\pm$ 1.1 GPa (Figure 2a,b). This corresponds to 101.7% and 170.8% improvements for σ and E compared with a pure ANF film, respectively. A further increase of the amounts of MWCNTs will result in the decrease of both E and σ (Figure 2a,b) due to the poor dispersion of MWCNTs when the loading is high.

Considering the flexibility of solution processing enabled by the colloidal nature of ANFs, we believe there is still a possibility to further the mechanical improvement. One of the challenges in the solution-based methods involving direct mixing such as VAF is the difficulty in retaining the nanoscale uniformity due to the phase separation, especially for composites with high filler contents. The LBL assembly technique stands out among other methods due to its higher accuracy enabled by the step-by-step deposition, avoiding the direct contact of different components in the solution state.[67,68] Compared with VAF, LBL assembly may result in nanocomposites with superior mechanical properties due to the better nanoscale organization and uniformity.[19,29] However, traditional LBL assembly is typically time-consuming, which necessitates some efforts to accelerate the process including exponential,[69] spray-assisted,[70] and spin-assisted LBL assembly techniques.[71] Here we performed LBL assembly on the filter paper assisted by vacuum to reduce the time for traditional LBL assembly and improve the mechanical properties of nanocomposites made by VAF. We filtered certain amounts of ANF and MWCNT dispersions alternatively, mimicking the LBL assembly process. Improvements of both stiffness (E) and ultimate strength (σ) were observed especially for higher loading of MWCNTs (Figure 3a,b). At a 5 wt % loading of MWCNTs, we achieved an E of 35.6 $\pm$ 1.4 GPa and a σ of 383 $\pm$ 8.1 MPa, respectively. The enhancement can be ascribed to the better dispersion state of MWCNTs in these vacuum-assisted LBL assembled composite films.[28]

Plotting the data collected from the literature and our results showed that ANF/MWCNT composite films exhibited superior properties to other CNT-based nanocomposites (both MWCNTs and SWCNTs) (Figure 3c). We further compared our results with that of GO-based nanocomposites for a more comprehensive evaluation (Figure 3d). Our composite films showed the best ultimate strength and overall improved integrated properties, which set ANF/MWCNT nanocomposites among the most strong and stiff carbon-based materials. It is also important to note that the achievement of such high mechanical performance at low loadings of MWCNTs can be very helpful for retaining the good transparency of ANF films (Figure 3e–g).

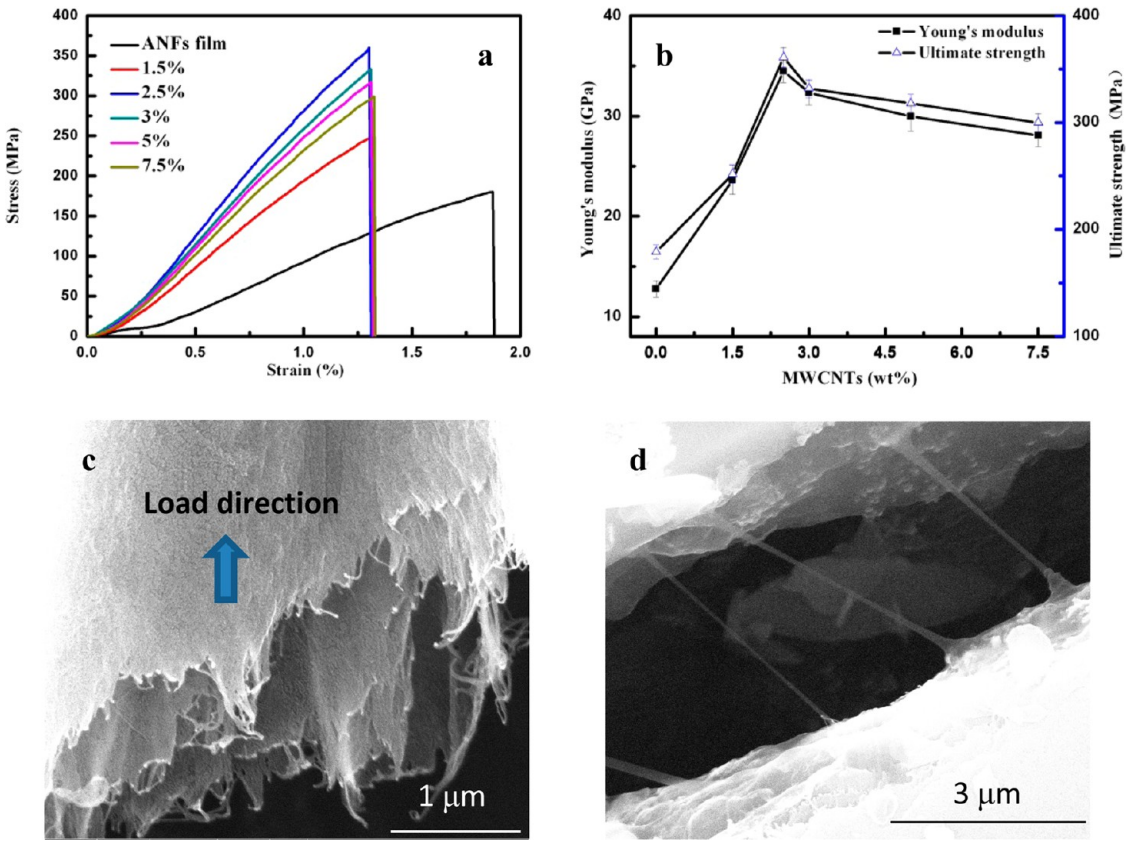

Figure 2. (a) Stress−strain curves of composite films with different amounts of MWCNTs; (b) variations of the ultimate strength and stiffness of composite films with different amounts of MWCNTs; SEM images of (c) a cracked surface and (d) an incomplete cracked surface from a composite film with 2.5 wt % MWCNTs.

We analyzed the cracks under load to understand the fracture process under tensile test. Fibrous structures consisting of both ANFs and MWCNTs can be found on the completely cracked surfaces (Figure 2c). A cracked part with some unbroken fibrous structures (Figure 2d) further indicated that during the crack growth not only MWCNTs but also ANFs may undergo elongation, breakage, and pull-out. The excellent mechanical properties of the nanoscale molecular assemblies possessed by ANFs can be therefore effectively utilized to prevent the crack growth, an obvious advantage over traditional polymers in single molecular states. Importantly, these processes are accompanied by multiple interactions between ANFs and MWCNTs, which result in a strong bonding interface (see below).

MWCNT and ANF Interactions. The construction of interfacial regions with strong interactions is an essential condition for the achievement of improved mechanical properties within nanocomposites especially for strength and stiffness.[28,29] A previous study indicated that the interfacial shear stress due to bonding could be as high as 500 MPa.[72] We believe the presence of multiple interactions may allow the effective strengthening and load transfer from ANFs to MWCNTs, resulting in high strength and stiffness. Compared with Kevlar macrofibers, ANFs possess a much larger surface area,[39] making possible the effective stress transfer between the typically inert high-strength polymer and CNTs. In addition to the interactions originated from surface functionalities, the aromatic structures within ANFs may also allow other intermolecular interactions with MWCNTs such as $\pi-\pi$ stacking (Figure 4a).

Indeed, we found that if the volume ratio of ANF and MWCNT DMSO dispersions (0.1 mg/mL) is more than 1:1, precipitation will be detected immediately, which is a good indicator for the strong interactions between functionalized MWCNTs and ANFs. We therefore reduced the additions of MWCNTs to avoid any detectable agglomerations. For the preparation of ANF/MWCNT nanocomposites, we added different amounts of MWCNT DMSO solutions (0.1 mg/mL) into ANF dispersions, which showed a dominant absorption around 400 nm with a less resolved broad peak around 320 nm (Figure 4b). Upon the addition of more MWCNTs, a continuous intensity decrease for the peak at 400 nm was observed along with the enhanced absorption at 320 nm. Similar spectral changes were detected upon the addition of water (Figure 4b inset). The peak at 400 nm can be associated with the absorption from the deprotonated ANFs, and the one around 320 nm is comparable with that of Kevlar macrofibers and correlated with the pronated ANFs.[39] We therefore attributed the absorption variations to the reprotonation of the negatively charged nitrogen

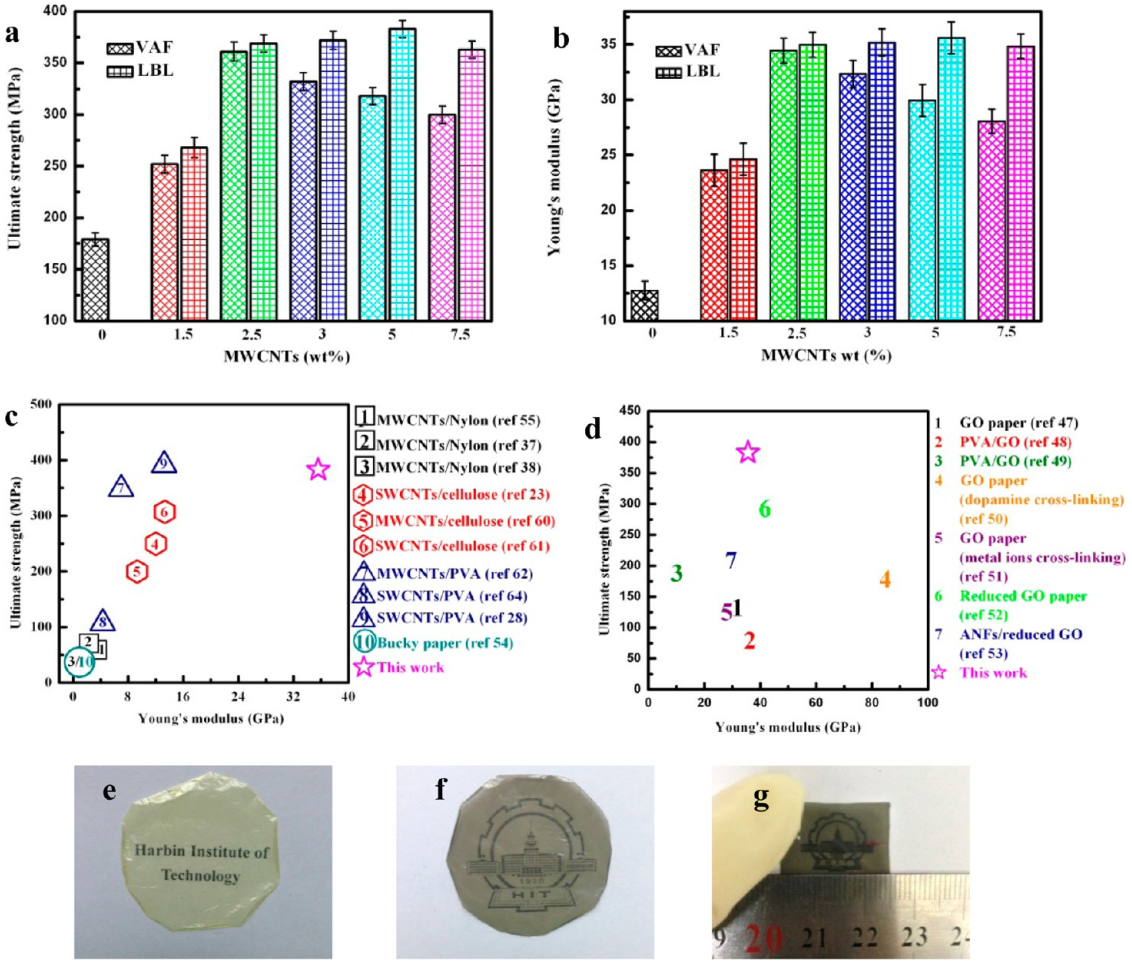

Figure 3. Comparisons of (a) ultimate strength and (b) Young's modulus of composite films made by VAF and vacuum-assisted LBL assembly; comparisons of ultimate strength and Young's modulus with (c) other CNT-based nanocomposites (both SWCNTs and MWCNTs) and (d) GO-based nanocomposites. The dashed borders in d identify regions with improving integrated properties. Optical images of (e) an ANF film and a composite film with (f) 2.5 wt % MWCNTs and (g) 5 wt % MWCNTs, respectively.

atoms on the surface of ANFs due to the interactions with −COOH groups on the surface of MWCNTs. Note that the peak at 400 nm can be detected for all the solution mixtures, indicating that ANFs are still partially charged, which is important for the stability of the system.

We further used IR spectra to probe the interactions between MWCNTs and ANFs (Figure 4c and d). Upon the addition of MWCNTs, peak broadenings around 1650 cm^{-1} (C═O stretching vibrations from ANFs) and around 3326 cm^{-1} (N−H stretching vibrations) were observed, which indicated the formation of hydrogen bonding with −COOH groups from MWCNTs. Further evidence of hydrogen bonding can be inferred from X-ray photoelectron spectroscopy (XPS) spectra.[73] The exclusive existence of nitrogen in ANFs ensured an accurate analysis of N_{1s} peaks, which are centered at 399.5 eV (Figure 5a). The addition of 2.5 wt % MWCNTs did not result in obvious changes (Figure 5b). However, for composite films with 5 and 7.5 wt % MWCNTs, N_{1s} peaks can be deconvoluted into two components, which include a high binding energy peak around 400.0 eV (Figure 5c,d). The intensity of this small peak also increases when more MWCNTs are present (Figure 5c,d). It is likely this new N_{1s} peak corresponds to nitrogen atoms that are involved in the interfacial hydrogen bonding.[73]

We further used Raman spectroscopy[74] to evaluate other possible interactions. The two main typical graphite bands are present in the Raman spectrum of bundled MWCNTs: the band at 1569 cm^{-1} (G band) assigned to the in-plane vibration of the C−C bond (G band) and the band at 1355 cm^{-1} (D band) activated by the presence of disorder in carbon systems (Figure 6a).[75] Both G and D bands for the MWCNT dispersion shifted to higher wavenumbers due to fewer intertube interactions (Figure 6a). It is hard to identify the obvious G and D bands for composite films due to the minimal amounts used (Figure 6a). However, we found that the strongest peak around 1610 cm^{-1} (C−C ring stretching of ANFs) underwent a gradual downshift upon the addition of more MWCNTs

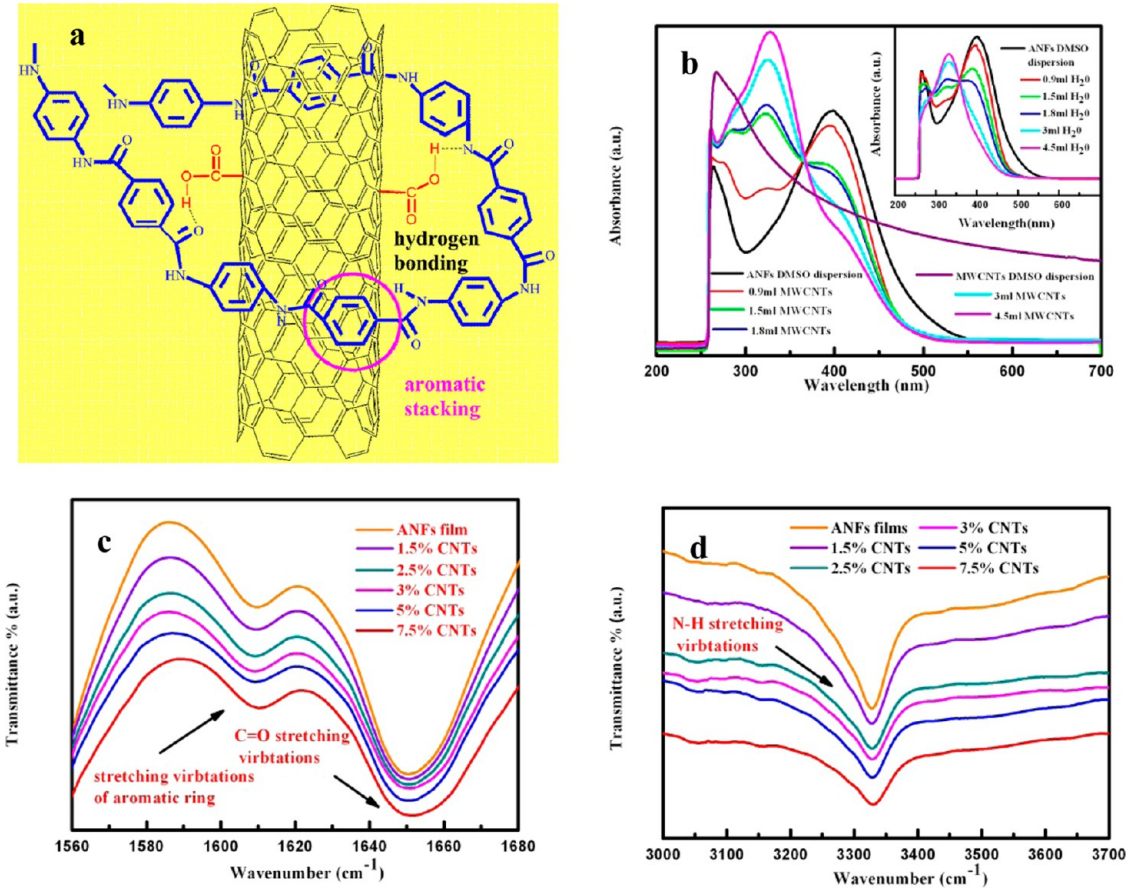

Figure 4. (a) Molecular structures of ANFs and CNTs showing the potential interactions including hydrogen bonding and $\pi-\pi$ stacking; (b) UV−vis spectra of ANFs with different additions of MWCNT DMSO dispersion (0.1 mg/mL); the inset shows the evolution of absorption upon the addition of different amounts of water; (c, d) IR spectra of composite films with different amounts of MWCNTs.

(Figure 6b). Such an observation can be direct evidence for the existence of $\pi-\pi$ interactions between ANFs and MWCNTs. Similar results have been observed for Raman shifts of the G band due to the charge transfer between the graphene sheets and large aromatic molecules.[76] To further confirm $\pi-\pi$ interactions, we investigated XPS spectra of C_{1s}. For ANFs, in addition to the peaks that can be assigned to −C−C−, −C−N−, and −CONH−, a broad peak around 290.3 eV arises from $\pi-\pi$ interactions of phenyl groups (Figure 7a).[77] Upon the addition of MWCNTs, this peak is gradually upshifted to 290.9 eV for composite films with 7.5 wt % MWCNTs (Figure 7d), which agrees with the results of Raman spectra.[76]

Microscopic observations showed that ANFs and MWCNTs have similar structural features with comparable nanoscale dimensions (the diameters of ANFs are ca. 10 nm and that of MWCNTs are ca. 40 nm; their lengths are both in the range of several micrometers) and good flexibility (Figure 8a,b). The size and geometry match of MWCNTs with ANFs can be very beneficial for achieving stronger materials due to the possible induced organization of polymers around carbon nanoparticle surfaces.[20] TEM imaging of the precipitation from ANFs and MWCNTs clearly showed the increase of surface roughness and diameters of the MWCNTs (Figure 8c,d). To achieve such tight coating, some morphology changes of ANFs forming sheet-like structures (see arrows in Figure 8c,d) were observed, which indirectly confirmed the strong interactions between ANFs and MWCNTs. Compared with MWCNTs that have a crystalline surface boundary (Figure 9a), the presence of ANFs resulted in an amorphous coating with a smooth interface (Figure 9b). This observation is different from previous studies using conjugated polymers in a molecular state, which resulted in the helical wrapping on the surface of the SWCNTs.[78]

Thermal and Thermomechanical Properties. Besides the excellent mechanical properties, the unique thermal and thermomechanical assets of ANFs further enable nanocomposites with high thermal stability and low coefficients of thermal expansion. ANF/MWCNT nanocomposites made by vacuum-assisted LBL assembly showed obvious weight losses starting from 520 °C (Figure 10a). The curve drop before 200 °C can be primarily attributed to the loss of water due to physical absorption. Larger weight losses for composite films with more MWCNTs were observed before 520 °C due

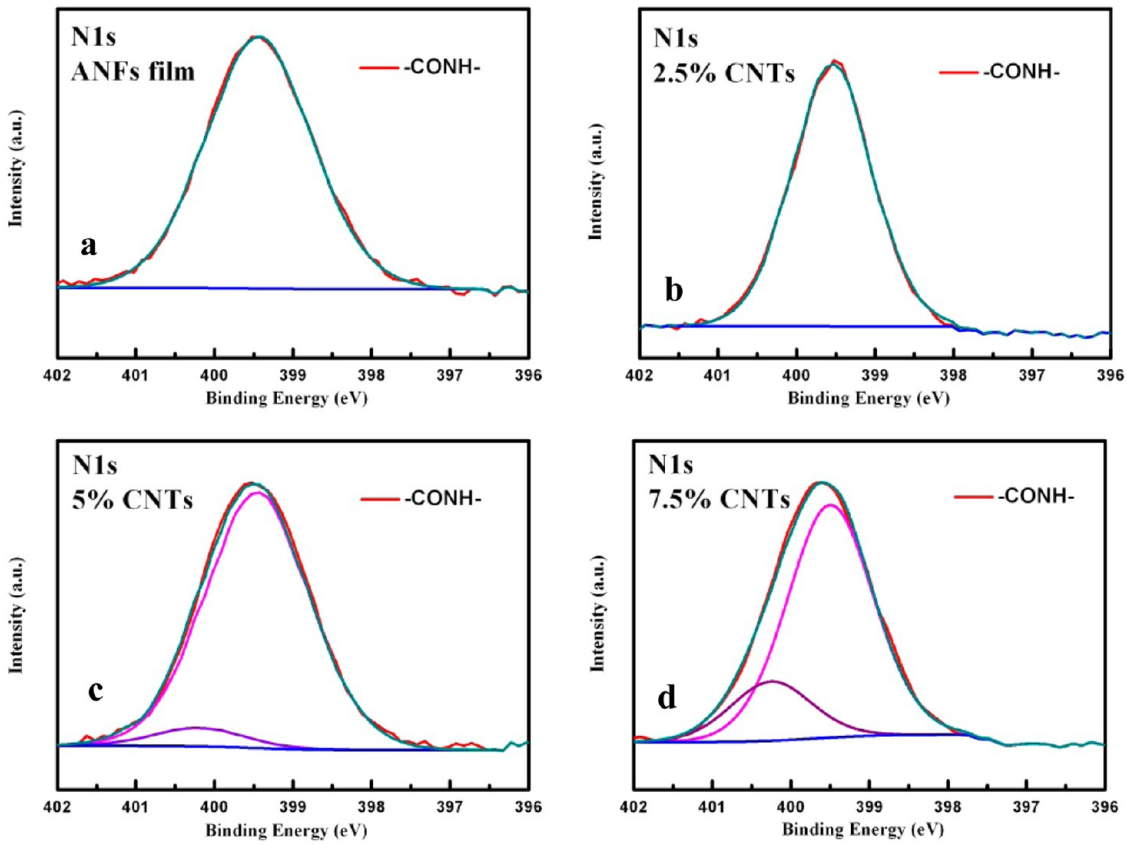

Figure 5. XPS N_{1s} spectra of (a) an ANF film and (b−d) composite films with different amounts of MWCNTs.

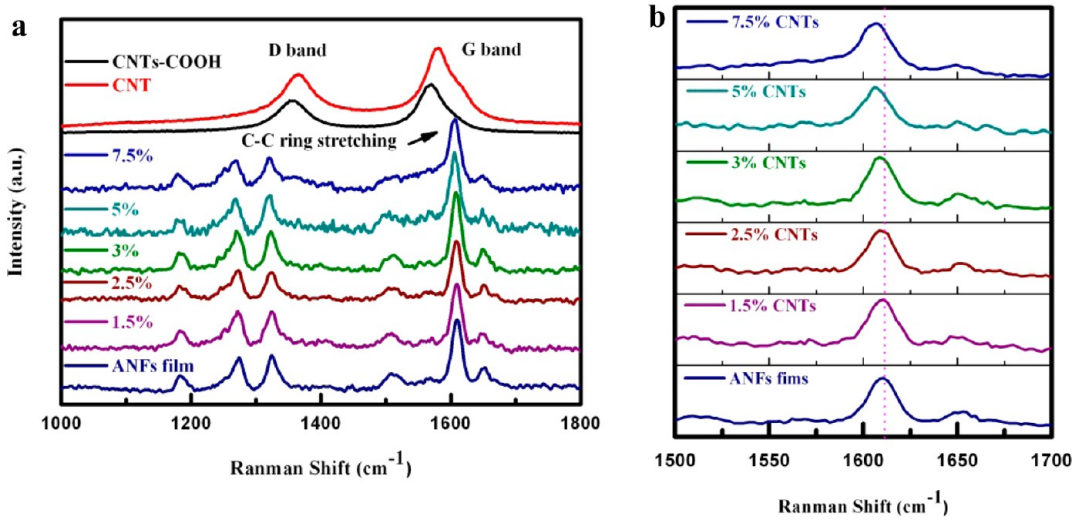

Figure 6. Raman spectra of an ANF film, composite films with different amounts of MWCNTs, −COOH-modified MWCNTs, and pristine MWCNTs.

to the decomposition of −COOH groups on the surface of MWCNTs (Figure S5). The high thermal stability of ANF/MWCNT composite films outperforms other CNT-based nanocomposites with high mechanical performance typically made from hydrophilic polymers such as PVA.[28]

We further investigated the thermomechanical properties by a thermal-mechanical analyzer. The CTE of the ANF film is 2.0 ppm·K^{-1} (Figure 10b,c), even smaller than that of cellulose nanofiber sheets, which was reported to be 8.5 ppm·K^{-1}.[79] We observed an increase of CTE upon the addition of more MWCNTs, different from most previous studies (Figure 10b,c).[80−85] The composite film with 7.5 wt % MWCNTs showed the largest CTE of 5.3 ppm·K^{-1}. One of the possible reasons for the increase of CTE

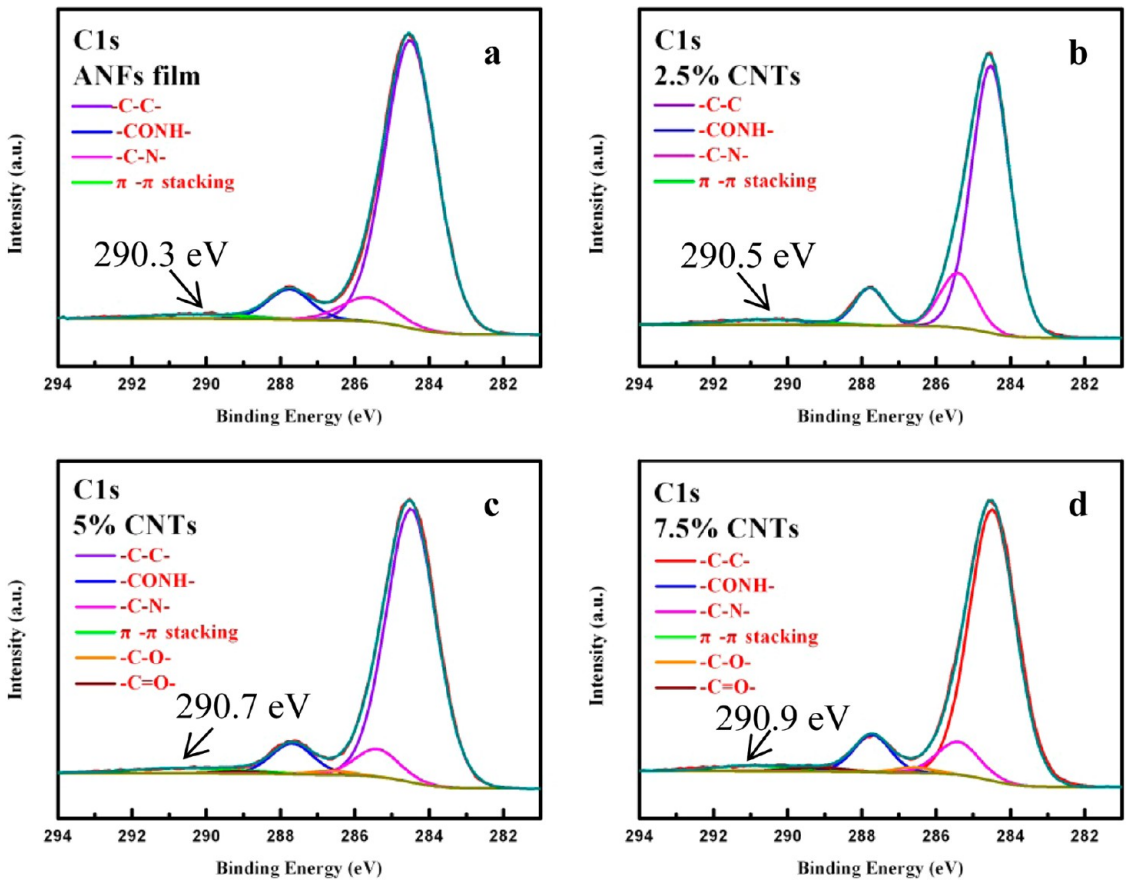

Figure 7. XPS C_{1s} spectra of (a) an ANFs film and (b−d) composite films with different amounts of MWCNTs.

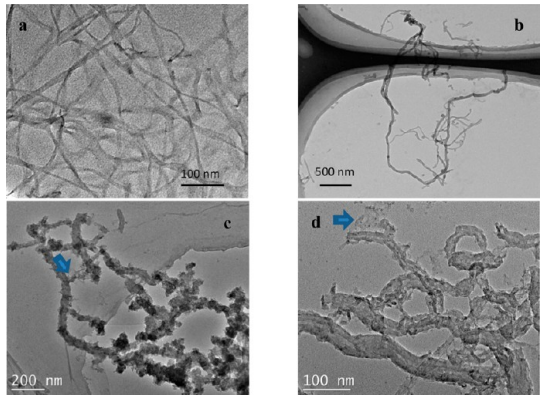

Figure 8. TEM images of (a) ANFs; (b) MWCNTs; and (c, d) ANF/MWCNT precipitations formed by adding MWCNTs into the DMSO dispersion of ANFs (the arrows indicate the sheet-like structures observed in this sample).

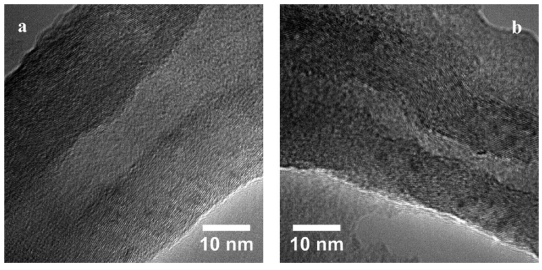

Figure 9. HRTEM images of (a) a MWCNT and (b) a MWCNT with ANFs.

could be the smaller CTE possessed by ANFs compared with that of MWCNTs, which was in the range 7.3−14.9 ppm·K^{-1}.[86] The origin of higher CTE as predicted by the MD theoretical study[87] may also be associated with the excluded volume induced by both the phonon modes and Brownian motions of the CNTs. However, considering the strong interactions between MWCNTs and ANFs, the excluded volume brought by the introduction of CNTs in our system may not be as important as in the simulated PE system.[87] The increases of CTE upon the change of temperature are small (Figure 10d), consistent with the linear displacement curve (Figure 10b). Overall, our preliminary CTE studies showed that ANF/MWCNT composite films have ultralow CTE (2−6 ppm·K^{-1}), which are several orders of magnitude smaller than other systems,[80−84] representing the lowest CTE when compared with previously reported MWCNT-based nanocomposites.

CONCLUSIONS

In summary, we showed that the incorporation of ANFs as new nanoscale building blocks into CNT-based

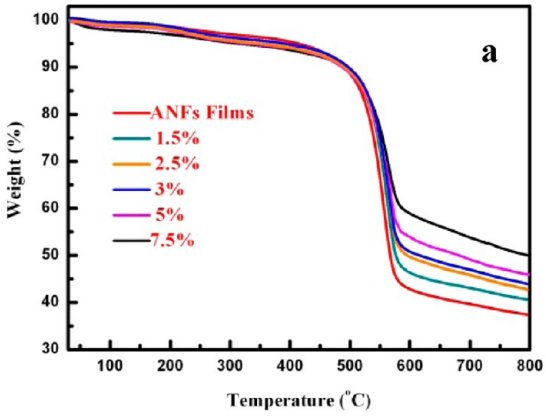

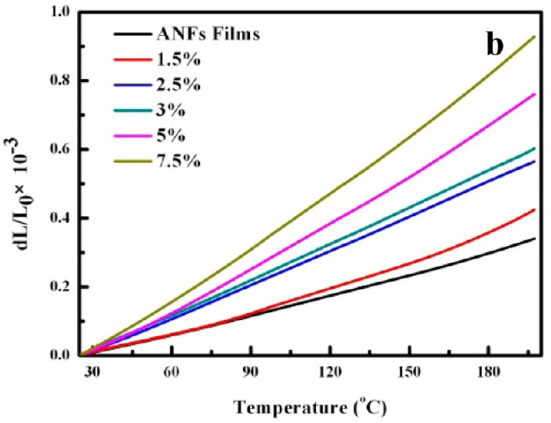

c

Samples	CTE(ppm·K^{-1}) (25-200℃)
ANFs film	2.0
1.5 %	2.5
2.5 %	3.3
3 %	3.5
5 %	4.4
7.5 %	5.3

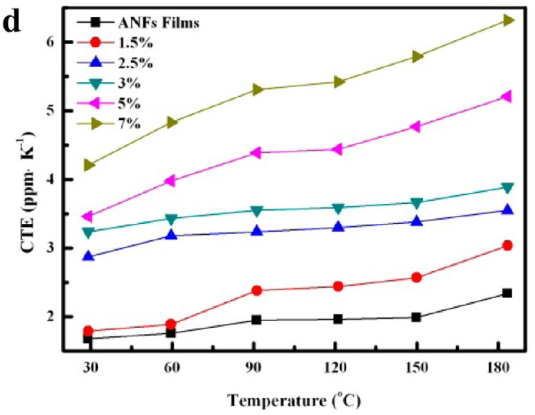

Figure 10. (a) TGA results, (b) relative length change from 25 to 200 °C, (c) a summary of CTE from 25 to 200 °C, and (d) temperature dependence of CTE for an ANF film and composite films with different amounts of MWCNTs.

nanocomposites can result in composite films with record-high ultimate strength and stiffness. The effective utilization of the outstanding mechanical properties of ANFs was made possible by the multiple interfacial interactions between ANFs and functionalized MWCNTs. ANFs also lend their intriguing thermal properties to the resulting hybrid materials with high thermal stability and ultralow coefficient of thermal expansion. We believe our work may provide a new concept for the design of high-performance polymeric nanocomposites, which can be applied to other nanoscale fillers such as clays and alumina platelets, resulting in a new class of composite materials with attractive multiparameter properties.

EXPERIMENTAL SECTION

Preparation of ANF DMSO Dispersions. Briefly, 1 g of bulk Kevlar yarns (Thread Exchange Inc., size 69, right twist) and 1.5 g of KOH were added into 500 mL of DMSO. The Kevlar/KOH/DMSO mixture was stirred vigorously at room temperature for a week before the formation of a dark red solution.

Preparation of MWCNT DMSO Dispersions. MWCNTs (purity, >95%; length, ~10 μm; and diameter, >40 nm) were purchased from Chengdu Organic Chemistry Co., Ltd. A 0.2 g amount of as-received MWCNTs was carefully added to a mixture of 90 mL concentrated sulfuric acid and 30 mL of concentrated nitric acid, followed by stirring for 4 h at 60 °C. The solution was diluted with a desired amount of deionized (DI) water before the collection of MWCNTs by vacuum filtration using a PVDF membrane (pore size, 0.22 μm; diameter, 47 cm). DI water was used to wash the MWCNT film to remove the excess amount of acids until the pH of the filtrates reached 7. After drying in a vacuum oven at 80 °C for 48 h, the as-obtained −COOH-functionalized MWCNTs can easily dissolve in DMSO, forming a homogeneous and stable dispersion assisted by ultrasonication at 350 W, 40 kHz for 60 min. The MWCNT DMSO dispersion was further centrifuged at 4000 rpm for 10 min to remove any possible bundles.

Preparation of ANF/MWCNT Composite Films. MWCNT and ANF DMSO dispersions were mixed with a given ratio followed by a desired amount of DI water to improve protonation. Briefly, 3 mL of ANF dispersion (2 mg/mL) was diluted to 30 mL by DMSO. Then MWCNT DMSO dispersions (0.1 mg/mL) of different volumes (0, 0.92, 1.54, 1.86, 3.16, and 4.86 mL corresponding to ANF films and composite films with 1.5%, 2.5%, 3%, 5%, and 7.5% MWCNTs, respectively) were added. For all mixtures, 4 mL of DI water was further added, which resulted in the formation of a gel-like structure. The color of the solutions turned from orange to yellow-white. The dispersions were stirred vigorously for 2 h by a turbine mixer to ensure a homogeneous mixture before vacuum filtration using nylon membranes with a 0.1 μm pore size (Beijing Afit Bioscience Co) at a vacuum pressure of −1 bar at room temperature. The vacuum-assisted LBL assembly mimicked the procedure of the traditional LBL assembly process. Briefly, the same volumes of ANF and MWCNT dispersions used during VAF were divided into 10 identical batches, respectively. The first batch of the ANF dispersion was filtered

followed by the first batch of the MWCNT dispersion. This process was repeated 10 times to achieve vacuum-assisted LBL assembled composite films, which were washed with DI water to eliminate impurities followed with air drying. Finally, they were peeled off from the membrane using a homemade tweezer. Thermal annealing of the composite films was conducted using a tube furnace at 200 °C in air for 1 h.

Instruments and Testing. TEM images were obtained on a transmission electron microscope (Tecnai G2 F20 S-Twin with 200 kV accelerating voltage of an electron beam). A dilution of the blend was deposited on an ultrathin carbon-coated copper grid and dried in an oven at 110 °C for 1 h before testing. Scanning electron microscopy (SEM) images were captured using a Quanta 200 (FEI, The Netherlands) machine with a 30 kV acceleration voltage. The cracked surface and cross-sectional images were obtained using samples singled out from the composite films after the mechanical tensile tests. For the observation of the incompletely cracked surface, we deliberately stopped the mechanical tensile test before the rupture. Atomic-force microscopy (AFM) experiments were performed in a tapping mode using a Dimension Icon atomic force microscope system (Veeco). The samples for AFM testing were prepared by immersing a PDDA-coated silicon wafer into a MWCNT dispersion followed by water rinsing and air drying.

Fourier transform infrared (FT-IR) spectra were recorded on a PerkinElmer Spectrum Frontier optical spectrometer. For the powder products, 1 wt % MWCNTs were pressed with KBr pellets and dried before FT-IR inspection. For film samples, they were immobilized on a fixture for convenient measurement directly. UV−vis spectra of the solutions were collected using a TU-1810 spectrophotometer with a resolution of 0.5 nm. NIR absorption spectra were obtained on a Hitachi U4100 spectrophotometer. X-ray diffraction measurements were performed on an X'Pert-Pro (Philips) using Cu Kα ($\lambda = 0.1541$ nm) generated at 40 kV and 100 mA with a scanning speed of 0.2° per min. Raman spectra were taken by an HR800 (JobinYvon, Inc.) machine with an excitation at 458 nm. The output power was set as 20 mW with a 30 s information acquisition time. X-ray photoelectron spectroscopy was performed using a PHI ESCA 5700 with Al Kα (1486.6 eV). Sputtering by Ar^+ under 1 μA and 300 eV for 2 min before testing is essential for accurate data.

A commercial nanotensile testing system (Nano UTM Universal Testing System T150, Agilent Technologies) with the method of "UTM-Bionix Standard Toecomp CDA" was used to conduct the tensile test. The maximum load and crosshead extension of this system are 500 mN and 150 mm, respectively. The samples were prepared as slender belts cut from films and fixed on perforated cardboard.The sizes of belt-like samples were measured by a caliper. Three individual samples of each category were prepared and tested. The tensile strain rate was set as 1.0×10^{-3} mm·s^{-1}. During the test, there is a sensitive spring that can provide a very small harmonic force (4.5 mN) with specific frequency (20 Hz) on the sample. Thus, the dynamic mechanical properties can be obtained during the tensile test.

The thermal properties of the composite films and MWCNTs were characterized by a thermogravimetric analyzer (TA Q500) using a heating rate of 10 °C/min from 30 to 800 °C under an atmosphere of nitrogen. Temperature sweep tests using a thermomechanical analyzer (TA Q400EM) were carried out from 25 to 200 °C with a heating rate of 10 °C/min. The coefficient of thermal expansion was determined with a 0.1 N preload on 8 mm long and 2 mm wide films during the second heating cycle.

The electrical conductivities were measured with a four-point probe Van der Pauw step using an Afilen E4980A tester. The dielectric properties were measured using an HP4192A RF impedance analysis tester with two fixed-size conductive silver electrodes on both surfaces of the films.

Conflict of Interest: The authors declare no competing financial interest.

Supporting Information Available: Characterization of −COOH MWCNT DMSO dispersion; SEM image of acid-treated MWCNTs; dynamic mechanical properties; TGA results for pristine MWCNTs and −COOH MWCNTs; electrical properties of ANF/MWCNT nanocomposites; percolation theory used for the determination of fc; summary of the ultimate strength and stiffness from different polymeric composite systems based on SWCNTs, MWCNTs, and GO. This material is available free of charge *via* the Internet at http://pubs.acs.org.

Acknowledgment. M.Y. would like to thank the National Natural Science Foundation of China (Grant No. 21303032), China Postdoctoral Science Foundation (Grant No. 2014M550184), HIT Young Talent Program (Grant No. AUGA5710050613), and Fundamental Research Funds for the Central Universities (Grant No. HIT. IBRSEM. A. 201406) for the financial support. Y. H. would like to thank the HIT 100-Talent Program (Grant No. AUGA5710006813) and Fundamental Research Funds for the Central Universities (Grant No. HIT IBRSEM. A. 201405) for the financial support. J.Z. would like to thank the National Natural Science Foundation of China (Grant No. 51222205) for the financial support. J.H. would like to thank the National Natural Science Foundation of China (Grant No. 11421091) for the financial support.

REFERENCES AND NOTES

1. Iijima, S.; Ichihashi, T. Single-Shell Carbon Nanotubes of 1-Nm Diameter. *Nature* **1993**, *363*, 603–605.
2. Yu, M. F.; Lourie, O.; Dyer, M. J.; Moloni, K.; Kelly, T. F.; Ruoff, R. S. Strength and Breaking Mechanism of Multiwalled Carbon Nanotubes under Tensile Load. *Science* **2000**, *287*, 637–640.
3. Moniruzzaman, M.; Winey, K. I. Polymer Nanocomposites Containing Carbon Nanotubes. *Macromolecules* **2006**, *39*, 5194–5205.
4. Coleman, J. N.; Khan, U.; Blau, W. J.; Gun'ko, Y. K. Small but Strong: A Review of the Mechanical Properties of Carbon Nanotube-Polymer Composites. *Carbon* **2006**, *44*, 1624–1652.
5. Baughman, R. H.; Zakhidov, A. A.; de Heer, W. A. Carbon Nanotubes - the Route toward Applications. *Science* **2002**, *297*, 787–792.
6. Ajayan, P. M.; Schadler, L. S.; Giannaris, C.; Rubio, A. Single-Walled Carbon Nanotube-Polymer Composites: Strength and Weakness. *Adv. Mater.* **2000**, *12*, 750.
7. Schadler, L. S.; Giannaris, S. C.; Ajayan, P. M. Load Transfer in Carbon Nanotube Epoxy Composites. *Appl. Phys. Lett.* **1998**, *73*, 3842–3844.
8. Salvetat, J. P.; Bonard, J. M.; Thomson, N. H.; Kulik, A. J.; Forro, L.; Benoit, W.; Zuppiroli, L. Mechanical Properties of Carbon Nanotubes. *Appl. Phys. A: Mater.* **1999**, *69*, 255–260.
9. Tasis, D.; Tagmatarchis, N.; Bianco, A.; Prato, M. Chemistry of Carbon Nanotubes. *Chem. Rev.* **2006**, *106*, 1105–1136.
10. Zhao, Y. L.; Stoddart, J. F. Noncovalent Functionalization of Single-Walled Carbon Nanotubes. *Acc. Chem. Res.* **2009**, *42*, 1161–1171.
11. Kim, S. W.; Kim, T.; Kim, Y. S.; Choi, H. S.; Lim, H. J.; Yang, S. J.; Park, C. R. Surface Modifications for the Effective Dispersion of Carbon Nanotubes in Solvents and Polymers. *Carbon* **2012**, *50*, 3–33.
12. Paiva, M. C.; Simon, F.; Novais, R. M.; Ferreira, T.; Proenca, M. F.; Xu, W.; Besenbacher, F. Controlled Functionalization of Carbon Nanotubes by a Solvent-Free Multicomponent Approach. *ACS Nano* **2010**, *4*, 7379–7386.
13. Hirsch, A. Functionalization of Single-Walled Carbon Nanotubes. *Angew. Chem., Int. Ed.* **2002**, *41*, 1853–1859.
14. Cheng, Q. F.; Bao, J. W.; Park, J.; Liang, Z. Y.; Zhang, C.; Wang, B. High Mechanical Performance Composite Conductor: Multi-Walled Carbon Nanotube Sheet/Bismaleimide Nanocomposites. *Adv. Funct. Mater.* **2009**, *19*, 3219–3225.
15. Dalton, A. B.; Collins, S.; Munoz, E.; Razal, J. M.; Ebron, V. H.; Ferraris, J. P.; Coleman, J. N.; Kim, B. G.; Baughman, R. H. Super-Tough Carbon-Nanotube Fibres - These Extraordinary Composite Fibres Can Be Woven into Electronic Textiles. *Nature* **2003**, *423*, 703–703.
16. Vigolo, B.; Penicaud, A.; Coulon, C.; Sauder, C.; Pailler, R.; Journet, C.; Bernier, P.; Poulin, P. Macroscopic Fibers and Ribbons of Oriented Carbon Nanotubes. *Science* **2000**, *290*, 1331–1334.

17. Wardle, B. L.; Saito, D. S.; Garcia, E. J.; Hart, A. J.; de Villoria, R. G.; Verploegen, E. A. Fabrication and Characterization of Ultrahigh-Volume-Fraction Aligned Carbon Nanotube-Polymer Composites. *Adv. Mater.* **2008**, *20*, 2707.
18. Cheng, Q. F.; Li, M. Z.; Jiang, L.; Tang, Z. Y. Bioinspired Layered Composites Based on Flattened Double-Walled Carbon Nanotubes. *Adv. Mater.* **2012**, *24*, 1838–1843.
19. Mamedov, A. A.; Kotov, N. A.; Prato, M.; Guldi, D. M.; Wicksted, J. P.; Hirsch, A. Molecular Design of Strong Single-Wall Carbon Nanotube/Polyelectrolyte Multilayer Composites. *Nat. Mater.* **2002**, *1*, 190–194.
20. Minus, M. L.; Chae, H. G.; Kumar, S. Single Wall Carbon Nanotube Templated Oriented Crystallization of Poly(Vinyl Alcohol). *Polymer* **2006**, *47*, 3705–3710.
21. Podsiadlo, P.; Tang, Z. Y.; Shim, B. S.; Kotov, N. A. Counterintuitive Effect of Molecular Strength and Role of Molecular Rigidity on Mechanical Properties of Layer-by-Layer Assembled Nanocomposites. *Nano Lett.* **2007**, *7*, 1224–1231.
22. Siro, I.; Plackett, D. Microfibrillated Cellulose and New Nanocomposite Materials: A Review. *Cellulose* **2010**, *17*, 459–494.
23. Koga, H.; Saito, T.; Kitaoka, T.; Nogi, M.; Suganuma, K.; Isogai, A. Transparent, Conductive, and Printable Composites Consisting of Tempo-Oxidized Nanocellulose and Carbon Nanotube. *Biomacromolecules* **2013**, *14*, 1160–1165.
24. Liu, T. X.; Phang, I. Y.; Shen, L.; Chow, S. Y.; Zhang, W. D. Morphology and Mechanical Properties of Multiwalled Carbon Nanotubes Reinforced Nylon-6 Composites. *Macromolecules* **2004**, *37*, 7214–7222.
25. Zhu, J.; Kim, J. D.; Peng, H. Q.; Margrave, J. L.; Khabashesku, V. N.; Barrera, E. V. Improving the Dispersion and Integration of Single-Walled Carbon Nanotubes in Epoxy Composites through Functionalization. *Nano Lett.* **2003**, *3*, 1107–1113.
26. Islam, M. F.; Rojas, E.; Bergey, D. M.; Johnson, A. T.; Yodh, A. G. High Weight Fraction Surfactant Solubilization of Single-Wall Carbon Nanotubes in Water. *Nano Lett.* **2003**, *3*, 269–273.
27. Haggenmueller, R.; Fischer, J. E.; Winey, K. I. Single Wall Carbon Nanotube/Polyethylene Nanocomposites: Nucleating and Templating Polyethylene Crystallites. *Macromolecules* **2006**, *39*, 2964–2971.
28. Shim, B. S.; Zhu, J.; Jan, E.; Critchley, K.; Ho, S. S.; Podsiadlo, P.; Sun, K.; Kotov, N. A. Multiparameter Structural Optimization of Single-Walled Carbon Nanotube Composites: Toward Record Strength, Stiffness, and Toughness. *ACS Nano* **2009**, *3*, 1711–1722.
29. Podsiadlo, P.; Kaushik, A. K.; Arruda, E. M.; Waas, A. M.; Shim, B. S.; Xu, J. D.; Nandivada, H.; Pumplin, B. G.; Lahann, J.; Ramamoorthy, A.; *et al.* Ultrastrong and Stiff Layered Polymer Nanocomposites. *Science* **2007**, *318*, 80–83.
30. Cranston, E. D.; Eita, M.; Johansson, E.; Netrval, J.; Salajkova, M.; Arwin, H.; Wagberg, L. Determination of Young's Modulus for Nanofibrillated Cellulose Multilayer Thin Films Using Buckling Mechanics. *Biomacromolecules* **2011**, *12*, 961–969.
31. Fox, J. D.; Capadona, J. R.; Marasco, P. D.; Rowan, S. J. Bioinspired Water-Enhanced Mechanical Gradient Nanocomposite Films That Mimic the Architecture and Properties of the Squid Beak. *J. Am. Chem. Soc.* **2013**, *135*, 5167–5174.
32. Shanmuganathan, K.; Capadona, J. R.; Rowan, S. J.; Weder, C. Biomimetic Mechanically Adaptive Nanocomposites. *Prog. Polym. Sci.* **2010**, *35*, 212–222.
33. Diez-Pascual, A. M.; Naffakh, M.; Marco, C.; Ellis, G.; Gomez-Fatou, M. A. High-Performance Nanocomposites Based on Polyetherketones. *Prog. Mater. Sci.* **2012**, *57*, 1106–1190.
34. Deng, F.; Ogasawara, T.; Takeda, N. Tensile Properties at Different Temperature and Observation of Micro Deformation of Carbon Nanotubes-Poly(Ether Ether Ketone) Composites. *Compos. Sci. Technol.* **2007**, *67*, 2959–2964.
35. Gao, J. B.; Itkis, M. E.; Yu, A. P.; Bekyarova, E.; Zhao, B.; Haddon, R. C. Continuous Spinning of a Single-Walled Carbon Nanotube-Nylon Composite Fiber. *J. Am. Chem. Soc.* **2005**, *127*, 3847–3854.
36. Kumar, S.; Dang, T. D.; Arnold, F. E.; Bhattacharyya, A. R.; Min, B. G.; Zhang, X. F.; Vaia, R. A.; Park, C.; Adams, W. W.; Hauge, R. H.; *et al.* Synthesis, Structure, and Properties of PBO/SWNT Composites. *Macromolecules* **2002**, *35*, 9039–9043.
37. Roh, S. C.; Kim, J.; Kim, C. K. Characteristics of Nylon 6,6/Nylon 6,6 Grafted Multi-Walled Carbon Nanotube Composites Fabricated by Reactive Extrusion. *Carbon* **2013**, *60*, 317–325.
38. Zhang, W. D.; Shen, L.; Phang, I. Y.; Liu, T. X. Carbon Nanotubes Reinforced Nylon-6 Composite Prepared by Simple Melt-Compounding. *Macromolecules* **2004**, *37*, 256–259.
39. Yang, M.; Cao, K. Q.; Sui, L.; Qi, Y.; Zhu, J.; Waas, A.; Arruda, E. M.; Kieffer, J.; Thouless, M. D.; Kotov, N. A. Dispersions of Aramid Nanofibers: A New Nanoscale Building Block. *ACS Nano* **2011**, *5*, 6945–6954.
40. Cao, K. Q.; Siepermann, C. P.; Yang, M.; Waas, A. M.; Kotov, N. A.; Thouless, M. D.; Arruda, E. M. Reactive Aramid Nanostructures as High-Performance Polymeric Building Blocks for Advanced Composites. *Adv. Funct. Mater.* **2013**, *23*, 2072–2080.
41. Chae, H. G.; Kumar, S. Rigid-Rod Polymeric Fibers. *J. Appl. Polym. Sci.* **2006**, *100*, 791–802.
42. Park, J. M.; Kim, D. S.; Kim, S. R. Improvement of Interfacial Adhesion and Nondestructive Damage Evaluation for Plasma-Treated PBO and Kevlar Fibers/Epoxy Composites Using Micromechanical Techniques and Surface Wettability. *J. Colloid Interface Sci.* **2003**, *264*, 431–445.
43. Jain, A.; Vijayan, K. Kevlar 49 Fibres: Thermal Expansion Coefficients from High Temperature X-Ray Data. *Curr. Sci. India* **2000**, *78*, 331–335.
44. O'Connor, I.; Hayden, H.; O'Connor, S.; Coleman, J. N.; Gun'ko, Y. K. Kevlar Coated Carbon Nanotubes for Reinforcement of Polyvinylchloride. *J. Mater. Chem.* **2008**, *18*, 5585–5588.
45. O'Connor, I.; Hayden, H.; O'Connor, S.; Coleman, J. N.; Gun'ko, Y. K. Polymer Reinforcement with Kevlar-Coated Carbon Nanotubes. *J. Phys. Chem. C* **2009**, *113*, 20184–20192.
46. Sainsbury, T.; Erickson, K.; Okawa, D.; Zonte, C. S.; Frechet, J. M. J.; Zettl, A. Kevlar Functionalized Carbon Nanotubes for Next-Generation Composites. *Chem. Mater.* **2010**, *22*, 2164–2171.
47. Dikin, D. A.; Stankovich, S.; Zimney, E. J.; Piner, R. D.; Dommett, G. H. B.; Evmenenko, G.; Nguyen, S. T.; Ruoff, R. S. Preparation and Characterization of Graphene Oxide Paper. *Nature* **2007**, *448*, 457–460.
48. Putz, K. W.; Compton, O. C.; Palmeri, M. J.; Nguyen, S. T.; Brinson, L. C. High-Nanofiller-Content Graphene Oxide-Polymer Nanocomposites *via* Vacuum-Assisted Self-Assembly. *Adv. Funct. Mater.* **2010**, *20*, 3322–3329.
49. Li, Y. Q.; Yu, T.; Yang, T. Y.; Zheng, L. X.; Liao, K. Bio-Inspired Nacre-Like Composite Films Based on Graphene with Superior Mechanical, Electrical, and Biocompatible Properties. *Adv. Mater.* **2012**, *24*, 3426–3431.
50. Tian, Y.; Cao, Y. W.; Wang, Y.; Yang, W. L.; Feng, J. C. Realizing Ultrahigh Modulus and High Strength of Macroscopic Graphene Oxide Papers through Crosslinking of Mussel-Inspired Polymers. *Adv. Mater.* **2013**, *25*, 2980–2983.
51. Park, S.; Lee, K. S.; Bozoklu, G.; Cai, W.; Nguyen, S. T.; Ruoff, R. S. Graphene Oxide Papers Modified by Divalent Ions - Enhancing Mechanical Properties *via* Chemical Cross-Linking. *ACS Nano* **2008**, *2*, 572–578.
52. Chen, H.; Muller, M. B.; Gilmore, K. J.; Wallace, G. G.; Li, D. Mechanically Strong, Electrically Conductive, and Biocompatible Graphene Paper. *Adv. Mater.* **2008**, *20*, 3557.
53. Fan, J. C.; Shi, Z. X.; Tian, M.; Yin, J. Graphene-Aramid Nanofiber Nanocomposite Paper with High Mechanical and Electrical Performance. *RSC Adv.* **2013**, *3*, 17664–17667.
54. Dettlaff-Weglikowska, U.; Skakalova, V.; Graupner, R.; Jhang, S. H.; Kim, B. H.; Lee, H. J.; Ley, L.; Park, Y. W.;

Berber, S.; Tomanek, D.; *et al*. Effect of Socl2 Treatment on Electrical and Mechanical Properties of Single-Wall Carbon Nanotube Networks. *J. Am. Chem. Soc.* **2005**, *127*, 5125–5131.
55. Chen, G. X.; Kim, H. S.; Park, B. H.; Yoon, J. S. Multi-Walled Carbon Nanotubes Reinforced Nylon 6 Composites. *Polymer* **2006**, *47*, 4760–4767.
56. Kim, K. T.; Jo, W. H. Non-Destructive Functionalization of Multi-Walled Carbon Nanotubes with Naphthalene-Containing Polymer for High Performance Nylon66/Multi-Walled Carbon Nanotube Composites. *Carbon* **2011**, *49*, 819–826.
57. Roy, S.; Das, T.; Ming, Y.; Chen, X. L.; Yue, C. Y.; Hu, X. Specific Functionalization and Polymer Grafting on Multiwalled Carbon Nanotubes to Fabricate Advanced Nylon 12 Composites. *J. Mater. Chem. A* **2014**, *2*, 3961–3970.
58. Saeed, K.; Park, S. Y. Preparation of Multiwalled Carbon Nanotube/Nylon-6 Nanocomposites by *in Situ* Polymerization. *J. Appl. Polym. Sci.* **2007**, *106*, 3729–3735.
59. Nogi, M.; Iwamoto, S.; Nakagaito, A. N.; Yano, H. Optically Transparent Nanofiber Paper. *Adv. Mater.* **2009**, *21*, 1595.
60. Salajkova, M.; Valentini, L.; Zhou, Q.; Berglund, L. A. Tough Nanopaper Structures Based on Cellulose Nanofibers and Carbon Nanotubes. *Compos. Sci. Technol.* **2013**, *87*, 103–110.
61. Hamedi, M. M.; Hajian, A.; Fall, A. B.; Hakansson, K.; Salajkova, M.; Lundell, F.; Wagberg, L.; Berglund, L. A. Highly Conducting, Strong Nanocomposites Based on Nanocellulose-Assisted Aqueous Dispersions of Single-Wall Carbon Nanotubes. *ACS Nano* **2014**, *8*, 2467–2476.
62. Coleman, J. N.; Cadek, M.; Blake, R.; Nicolosi, V.; Ryan, K. P.; Belton, C.; Fonseca, A.; Nagy, J. B.; Gun'ko, Y. K.; Blau, W. J. High-Performance Nanotube-Reinforced Plastics: Understanding the Mechanism of Strength Increase. *Adv. Funct. Mater.* **2004**, *14*, 791–798.
63. Bhattacharyya, S.; Salvetat, J. P.; Saboungi, M. L. Reinforcement of Semicrystalline Polymers with Collagen-Modified Single Walled Carbon Nanotubes. *Appl. Phys. Lett.* **2006**, *88*, 233119.
64. Liu, L. Q.; Barber, A. H.; Nuriel, S.; Wagner, H. D. Mechanical Properties of Functionalized Single-Walled Carbon-Nanotube/Poly(Vinyl Alcohol) Nanocomposites. *Adv. Funct. Mater.* **2005**, *15*, 975–980.
65. Zhang, X. F.; Liu, T.; Sreekumar, T. V.; Kumar, S.; Moore, V. C.; Hauge, R. H.; Smalley, R. E. Poly(Vinyl Alcohol)/SWNT Composite Film. *Nano Lett.* **2003**, *3*, 1285–1288.
66. Feng, W.; Bai, X. D.; Lian, Y. Q.; Liang, J.; Wang, X. G.; Yoshino, K. Well-Aligned Polyaniline/Carbon-Nanotube Composite Films Grown by in-Situ Aniline Polymerization. *Carbon* **2003**, *41*, 1551–1557.
67. Hammond, P. T. Form and Function in Multilayer Assembly: New Applications at the Nanoscale. *Adv. Mater.* **2004**, *16*, 1271–1293.
68. Decher, G. Fuzzy Nanoassemblies: Toward Layered Polymeric Multicomposites. *Science* **1997**, *277*, 1232–1237.
69. Li, Y.; Wang, X.; Sun, J. Q. Layer-by-Layer Assembly for Rapid Fabrication of Thick Polymeric Films. *Chem. Soc. Rev.* **2012**, *41*, 5998–6009.
70. Schaaf, P.; Voegel, J. C.; Jierry, L.; Boulmedais, F. Spray-Assisted Polyelectrolyte Multilayer Buildup: From Step-by-Step to Single-Step Polyelectrolyte Film Constructions. *Adv. Mater.* **2012**, *24*, 1001–1016.
71. Kharlampieva, E.; Kozlovskaya, V.; Chan, J.; Ankner, J. F.; Tsukruk, V. V. Spin-Assisted Layer-by-Layer Assembly: Variation of Stratification as Studied with Neutron Reflectivity. *Langmuir* **2009**, *25*, 14017–14024.
72. Wagner, H. D.; Lourie, O.; Feldman, Y.; Tenne, R. Stress-Induced Fragmentation of Multiwall Carbon Nanotubes in a Polymer Matrix. *Appl. Phys. Lett.* **1998**, *72*, 188–190.
73. Liu, S. Y.; Chan, C. M.; Weng, L. T.; Li, L.; Jiang, M. Surface Characterization of Poly(Styrene-co-P-Hexafluorohydroxy-isopropyl-Alpha-Methylstyrene)/Poly(4-Vinylpyridine) Blends Spanning the Immiscibility-Miscibility-Complexation Transition by XPS, TOF-SIMS, and AFM. *Macromolecules* **2002**, *35*, 5623–5629.
74. Dresselhaus, M. S.; Dresselhaus, G.; Saito, R.; Jorio, A. Raman Spectroscopy of Carbon Nanotubes. *Phys. Rep.* **2005**, *409*, 47–99.
75. Bokobza, L.; Zhang, J. Raman Spectroscopic Characterization of Multiwall Carbon Nanotubes and of Composites. *Express Polym. Lett.* **2012**, *6*, 601–608.
76. Su, Q.; Pang, S. P.; Alijani, V.; Li, C.; Feng, X. L.; Mullen, K. Composites of Graphene with Large Aromatic Molecules. *Adv. Mater.* **2009**, *21*, 3191.
77. SalehiMobarakeh, H.; AitKadi, A.; Brisson, J. Improvement of Mechanical Properties of Composites through Polyamide Grafting onto Kevlar Fibers. *Polym. Eng. Sci.* **1996**, *36*, 778–785.
78. Zhu, J.; Shim, B. S.; Di Prima, M.; Kotov, N. A. Transparent Conductors from Carbon Nanotubes LBL-Assembled with Polymer Dopant with Pi-Pi Electron Transfer. *J. Am. Chem. Soc.* **2011**, *133*, 7450–7460.
79. Nogi, M.; Yano, H. Optically Transparent Nanofiber Sheets by Deposition of Transparent Materials: A Concept for a Roll-to-Roll Processing. *Appl. Phys. Lett.* **2009**, *94*, 233117.
80. Xu, Y. S.; Ray, G.; Abdel-Magid, B. Thermal Behavior of Single-Walled Carbon Nanotube Polymer-Matrix Composites. *Compos. Part. A: Appl. S* **2006**, *37*, 114–121.
81. Abdalla, M.; Dean, D.; Theodore, M.; Fielding, J.; Nyairo, E.; Price, G. Magnetically Processed Carbon Nanotube/Epoxy Nanocomposites: Morphology, Thermal, and Mechanical Properties. *Polymer* **2010**, *51*, 1614–1620.
82. Wang, S. R.; Liang, Z. Y.; Gonnet, P.; Liao, Y. H.; Wang, B.; Zhang, C. Effect of Nanotube Functionalization on the Coefficient of Thermal Expansion of Nanocomposites. *Adv. Funct. Mater.* **2007**, *17*, 87–92.
83. dos Santos, A. S.; Leite, T. D. N.; Furtado, C. A.; Welter, C.; Pardini, L. C.; Silva, G. G. Morphology, Thermal Expansion, and Electrical Conductivity of Multiwalled Carbon Nanotube/Epoxy Composites. *J. Appl. Polym. Sci.* **2008**, *108*, 979–986.
84. Huang, J. M.; Tsai, M. F.; Yang, S. J.; Chiu, W. M. Preparation and Thermal Properties of Multiwalled Carbon Nanotube/Polybenzoxazine Nanocomposites. *J. Appl. Polym. Sci.* **2011**, *122*, 1898–1904.
85. Nogi, M.; Ifuku, S.; Abe, K.; Handa, K.; Nakagaito, A. N.; Yano, H. Fiber-Content Dependency of the Optical Transparency and Thermal Expansion of Bacterial Nanofiber Reinforced Composites. *Appl. Phys. Lett.* **2006**, *88*, 133124.
86. Wu, F. Y.; Cheng, H. M. Structure and Thermal Expansion of Multi-Walled Carbon Nanotubes before and after High Temperature Treatment. *J. Phys. D. Appl. Phys.* **2005**, *38*, 4302–4307.
87. Wei, C. Y.; Srivastava, D.; Cho, K. J. Thermal Expansion and Diffusion Coefficients of Carbon Nanotube-Polymer Composites. *Nano Lett.* **2002**, *2*, 647–650.